IEEE Access
Multidisciplinary ⋮ Rapid Review ⋮ Open Access Journal

Received 11 June 2024, accepted 3 July 2024, date of publication 17 July 2024, date of current version 29 July 2024.

Digital Object Identifier 10.1109/ACCESS.2024.3430216

RESEARCH ARTICLE

A New Design Approach for Dual-Band Quadrature Hybrids With Practically Unlimited Band Ratio, Enhanced Power Division, and Arbitrary Port Impedance

AHAMMAD[1], (Graduate Student Member, IEEE), ASIF IFTEKHAR OMI[2], (Student Member, IEEE), MOHAMMAD H. MAKTOOMI[3], (Graduate Student Member, IEEE), MOHAMMAD A. MAKTOOMI[4], (Member, IEEE), AND PRAVEEN K. SEKHAR[1], (Member, IEEE)

[1]Department of Engineering and Computer Science, Washington State University Vancouver, Vancouver, WA 98686, USA
[2]Department of Electrical and Computer Engineering, University of Florida, Gainesville, FL 32611, USA
[3]Department of Electrical and Computer Engineering, University of California at Irvine, Irvine, CA 92697, USA
[4]Department of Electrical and Computer Engineering, Virginia Military Institute, Lexington, VA 24450, USA

Corresponding author: Praveen K. Sekhar (praveen.sekhar@wsu.edu)

This work was supported in part by the National Science Foundation under Grant 2104513.

ABSTRACT This paper introduces a novel design methodology for a dual-band branch-line coupler (DBBLC) that, for the first time, facilitates practically unlimited band ratio, enhanced flexibility in power division, and arbitrary port termination impedance concurrently. This approach ensures precise power distribution, matching, and isolation requirements by utilizing a generalized coupler core paired with an L-section impedance-matching network. This paper details an innovative and comprehensive analytical strategy for DBBLC design, which overcomes the limitations noted in prior research by deriving a generalized formula for the power division ratio (k) and simplifying the design equations to decrease complexity. This method enables the simultaneous realization of varied power division ratios, frequency ratios (r), and port impedances (Z_p), thus offering remarkable design versatility. The effectiveness of this new analytical design methodology is corroborated through several design examples. Moreover, two prototype models operating at 1 GHz/2.5 GHz ($r = 2.5$, $k = 0$ dB) and 1 GHz/2 GHz ($r = 2$, $k = 4.77$ dB) frequencies, constructed on Rogers' RO4003C substrate, exhibit > 22 dB return loss, < 0.64 dB amplitude imbalance as well as $< 1°$ phase imbalance of the transmission parameters and > 25 dB isolation at all the targeted frequencies. Therefore, the development and validation of this new DBBLC structure, as demonstrated by the strong correlation between our simulated and experimental findings, not only surpasses the capabilities of existing models, but also broadens the applicability of dual-band couplers in modern wireless communication systems.

INDEX TERMS Branch-line coupler, dual-band, impedance matching, microwave, power divider, quadrature, RF.

I. INTRODUCTION

The Branch-Line Coupler (BLC) is a ubiquitous component required for next generation wireless systems and technologies [1]. In recent years, dual-band/multiband and

The associate editor coordinating the review of this manuscript and approving it for publication was Qi Luo.

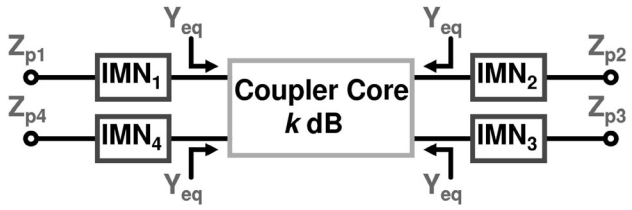

FIGURE 1. The generalized BLC structure.

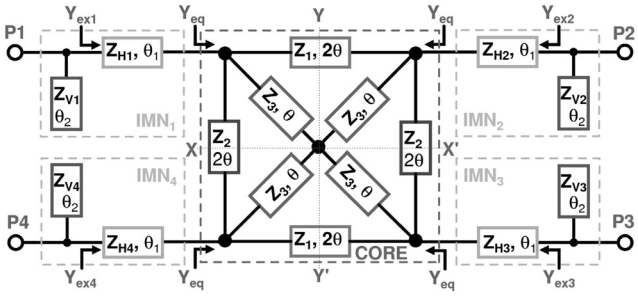

FIGURE 2. The proposed diagonally crossed TL based DBBLC.

reconfigurable components have gained paramount importance because of their potential use in cognitive/software-defined radios [2], [3], [4], [5], [6]. The demand for dual-band/multi-band and re-configurable components in recent years has paved the way for the rapid development of numerous dual-band BLCs (DBBLCs) with high-end capabilities for power combining/splitting in various applications such as multistage and Doherty power amplifiers (PA) [7], mixers [8], beam forming networks [9], and other RF front-end systems [10], [11], [12]. Replacing all the quarter-wave lines of a conventional single-band BLC with equivalent dual-band composite right/left-hand transmission lines (TLs), Pi/T-networks, coupled lines, crossed lines, and stepped impedance with open/short stub lines gives rise to dual-band BLC structures [13], [14], [15], [16], [17], [18], [19], [20], [21], [22], [23], [24]. However, the reported designs have limited band-ratios [13], [14], complex design procedures [15], [16], [17] or offer only equal/unequal power division [18], [19], [20], [21], [22], [23]. The current state-of-the-art designs cannot simultaneously support arbitrary port impedances, higher band ratios, and arbitrary power divisions. The design of such devices is challenging.

Recent studies, such as those reported in [25] and [26], have introduced innovative design concepts for generalized DBBLCs with unequal power division and arbitrary port terminations. However, these studies exhibited significant limitations, including the absence of a generalized equation for the power division ratio (k), an undetermined maximum achievable band ratio (r_{max}), and the complexity introduced by using two-section transmission lines as matching networks at port terminations. These constraints restrict the versatility and applicability of design methodologies, confining them to specific structures rather than providing a broadly applicable solution.

Similarly, the works in [20] and [27] applied Riblet's technique to the dual-band scenario, achieving simpler design equations compared to conventional dual-band port-extended couplers. Despite these improvements, these designs also lack a generalized power division ratio (k) and rely on complex two-section transmission lines with open/short stubs to enhance k and r, further complicating the design process. Consequently, these methodologies are not generalizable, and are tailored to specific BLC structures.

Furthermore, the design approach in [13] utilizes cross-coupling branches in conventional branch hybrid couplers but fails to address the power division ratio (k), limiting its application to equal power division scenarios and constraining the frequency ratio (r). The design methodologies presented in these studies are specific to the reported structures and lack the flexibility required for broader applications.

In contrast, this study introduces a novel and comprehensive analytical method for designing dual-band branch-line couplers (DBBLCs)to address and overcome the limitations identified in previous studies. This approach includes deriving a generalized formulation for the power division ratio (k) and developing simpler design equations that eliminate the complexity associated with using two-section transmission lines at port termination. This methodology enables the simultaneous achievement of arbitrary power division ratios (k), frequency ratios (r), and port impedances (Z_p), offering unprecedented design flexibility. To the best of the authors' knowledge, this is the first instance where such versatility and simplicity have been demonstrated in DBBLC design, setting the work apart from existing references providing significant advancements in the field, and establishing a robust framework for future DBBLC designs.

This paper proposes a unique design methodology for generalized branch-line coupler (BLC) structures comprising a core part and an impedance matching network (IMN), as shown in Fig.1. A detailed theoretical analysis was conducted to derive closed-form design equations to determine the parameters of the coupling structure. The versatility of the presented approach is substantiated by several key contributions reported for the first time to the best of the authors' knowledge: (a) the derivation of a universal power division ratio applicable to any BLC core structure and (b) the formulation of a systematic approach for achieving virtually unlimited band ratios, extreme power division, and arbitrary port impedance simultaneously.

Although the proposed methodology is generic, for demonstration purposes, we chose a basic BLC with diagonally intersecting transmission lines (TLs) as the core structure, coupled with an easy-to-analyze L-section matching circuit as the IMN, as shown in Fig. 2. This configuration effectively shows the proposed novelties and supports multiple unique features within the overall structure. Through this example, the practical application and superior flexibility of the design

method are illustrated, highlighting its potential for broad applicability in advanced microwave circuit design.

II. PROPOSED DESIGN METHODOLOGY

The theory starts by analyzing the generic BLC structure shown in Fig. 1, and a practical implementation is shown in Fig. 2.

A. NEW EQUATION FOR POWER DIVISION RATIO K

For the generalized BLC structure shown in Fig. 2, the equivalent input admittance at any port of the coupler core is denoted as $Y_{eq} = G_{eq} + jB_{eq}$ where G_{eq} and B_{eq} represent the equivalent input conductance and susceptance of the coupler, respectively. When the coupler core is terminated with Y^*_{eq}, the generalized S-parameter equations listed in Eqs. (1)-(4) of [22] hold true.

$$S_{11} = \frac{1}{4}(\Gamma_{ee} + \Gamma_{eo} + \Gamma_{oe} + \Gamma_{oo}) \tag{1}$$

$$S_{21} = \frac{1}{4}(\Gamma_{ee} - \Gamma_{eo} + \Gamma_{oe} - \Gamma_{oo}) \tag{2}$$

$$S_{31} = \frac{1}{4}(\Gamma_{ee} - \Gamma_{eo} - \Gamma_{oe} + \Gamma_{oo}) \tag{3}$$

$$S_{41} = \frac{1}{4}(\Gamma_{ee} + \Gamma_{eo} - \Gamma_{oe} - \Gamma_{oo}) \tag{4}$$

If we denote the generalized susceptance of its even-even, odd-odd, odd-even, and even-odd mode equivalent circuits as B_A, B_B, B_C, and B_D, respectively, then by setting $S_{11} = 0$ and $S_{41} = 0$, the equations related to G_{eq}, and B_{eq} can be obtained as:

$$(G^2_{eq} + B^2_{eq}) - B_{eq}(B_A + B_D) + B_A B_D = 0 \tag{5}$$

$$(G^2_{eq} + B^2_{eq}) - B_{eq}(B_B + B_C) + B_B B_C = 0 \tag{6}$$

Solving (5) and (6) simultaneously yields:

$$G_{eq} = \frac{\sqrt{(B_C - B_A)(B_C - B_D)(B_B - B_A)(B_D - B_B)}}{B_A + B_D - B_B - B_C} \tag{7}$$

$$B_{eq} = \frac{B_A B_D - B_B B_C}{B_A + B_D - B_B - B_C} \tag{8}$$

The ratios of S_{21} and S_{31} of the coupler are related to the power division parameter k, (k > 0) as follows [22]:

$$\frac{S_{21}}{S_{31}} = \frac{\Gamma_{ee} - \Gamma_{oo}}{\Gamma_{ee} + \Gamma_{oo}} = ke^{-j\frac{\pi}{2}} \tag{9}$$

Here, $20log|k|$ denotes the power division ratio in decibels. The reflection coefficients Γ_{ij} ($i = \{o, e\}$ and $j = \{o, e\}$) for all even and odd cases are given by:

$$\Gamma_{ij} = \frac{Y_{eq} - Y_{ij}}{Y^*_{eq} + Y_{ij}} \left(\frac{Y^*_{eq}}{Y_{eq}}\right), \{i, j\} = \{e, o\} \tag{10}$$

Combining (10) with (9) yields the generalized k:

$$k = \sqrt{\frac{(B_B - B_A)(B_C - B_D)}{(B_C - B_A)(B_D - B_B)}} \tag{11}$$

It is apparent that k depends only on B_A to B_D, which are functions of the characteristic impedances of the BLC core TLs, Z_c where $c = \{1, 2, 3 \ldots, n\}$. The generalized k paves the way for obtaining design parameters for any DBBLC structure.

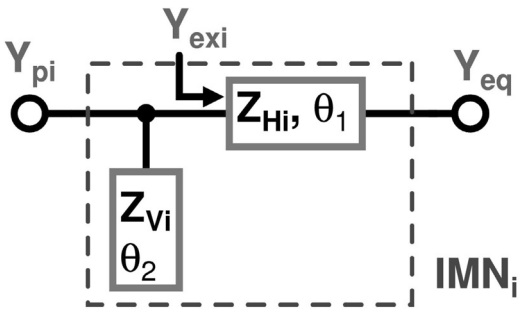

FIGURE 3. Configuration of an L-section IMN.

B. SYSTEMATIC DESIGN FORMULATION FOR ANY DBBLC

For any value of k, when identical IMNs are added to match Y_{eq} with the port-termination impedance, the entire structure acts as a quadrature hybrid. In dual-band designs, the electrical length and frequency are interdependent [17]. If the design frequencies are f_1 and f_2, where $f_2 > f_1$ and the dual-band ratio is $r = f_2/f_1$, then the electrical lengths at f_1 for dual-band cases can be obtained as

$$\theta|_{f_1} = \frac{m\pi}{1 + r} = tan^{-1}a \tag{12}$$

$$\theta_1|_{f_1} = \frac{p\pi}{1 + r} = tan^{-1}a_1 \tag{13}$$

$$\theta_2|_{f_1} = \frac{q\pi}{1 + r} = tan^{-1}a_2 \tag{14}$$

where the electrical length of all the core transmission lines (TLs) is θ, the L-section and IMN comprise TLs with electrical lengths θ_1 and θ_2, respectively. m, p, q are positive integers.

Thus, from the equations above, when r increases, the fundamental electrical length $\pi/(1 + r)$ decreases. Accordingly, even if m, p, and q increased, the electrical lengths ($\theta, \theta_1, \theta_2$) were not significantly affected. Practically, these electrical lengths are always in the realizable range because the stubs can always be folded in the vacant PCB space available in the vicinity of each port. To clarify the maxima/minima of stub sizes, inequality (15) has been added, which ensures these realizable electrical lengths. It is worth noting that for $r > 10$, (15) was used to ensure realizable values of the electrical lengths for all TLs. Moreover, the entire manuscript discusses all TL impedances limited between 20Ω and 120Ω. All the plots have been generated by enforcing this limit, so that the line impedances cannot cross this boundary.

$$\frac{r + 1}{9} < m, p, q < \frac{r + 1}{3} \tag{15}$$

In this study, basic L-section IMNs are used to match the resulting $Y_{eq} = G_{eq} + jB_{eq}$ from (7) and (8) to port termination impedances, Z_{pi} (normally $Z_{p1} = Z_{p2} = Z_{p3} = Z_{p4} = Z_p =$

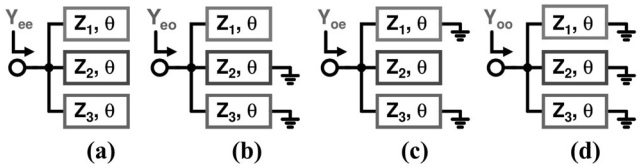

FIGURE 4. Equivalent (a) even-even (b) even-odd (c) odd-even (d) odd-odd configurations for DBBLC core shown in Fig. 2.

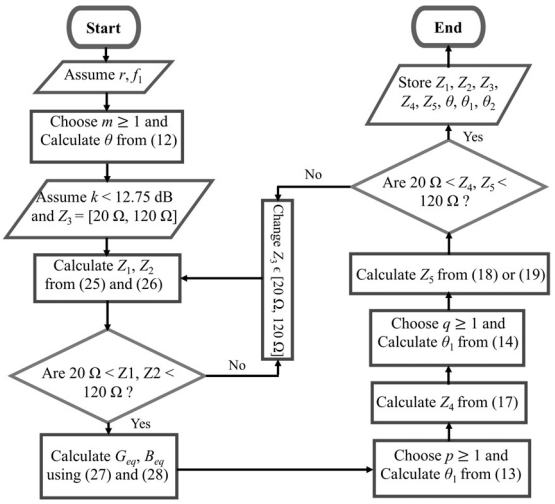

FIGURE 5. Flowchart demonstrating the novel design approach.

50Ω) thereby regulating $S_{ii}, i = \{1, 2, 3, 4\}$. As shown in Fig. 3, the (Z_{Hi}, θ_1) TL transfers Y_{eq} to Y_{exi}, where:

$$Y_{exi} = G_{exi} + jB_{exi} \tag{16}$$

Setting $G_{exi} = 1/Z_{pi}$, we get:

$$Z_{Hi} = \frac{(1 + a_1^2)G_{eq} - Y_{pi}}{\sqrt{(2a_1 Y_{pi} B_{eq})^2 + \{(1+a_1^2)G_{eq} - Y_{pi}\}Y_{pi}a_1^2|Y_{eq}|^2} - a_1 Y_{pi} B_{eq}} \tag{17}$$

A realizable solution of Z_{Hi} from (17) equalizes G_{exi} to port termination admittance $Y_{pi} = 1/Z_{pi}$. The susceptance B_{exi} can be canceled using an open- or short-circuit stub, whose characteristic impedance Z_{Vi} is calculated as follows:

$$Z_{Vi(open)} = \frac{a_2[(Y_{Hi} - a_1 B_{eq})^2 + a_1^2 G_{eq}^2]}{Y_{Hi}[a_1(|Y_{eq}|^2 + Y_{Hi}^2) - B_{eq} Y_{Hi}(1 - a_1^2)]} \tag{18}$$

$$Z_{Vi(short)} = \frac{[(Y_{Hi} - a_1 B_{eq})^2 + a_1^2 G_{eq}^2]}{a_2 Y_{Hi}[B_{eq} Y_{Hi}(1 - a_1^2) - a_1(|Y_{eq}|^2 + Y_{Hi}^2)]} \tag{19}$$

By using the derived closed-form equations in this section, we can design any DBBLC for arbitrary r, k and Z_{pi} using the following design steps.

a) Choose a suitable k dB core section.

b) Calculate θ, θ_1 and θ_2 from (12)-(14), along with suitable values of m, p, and q dictated by (15).

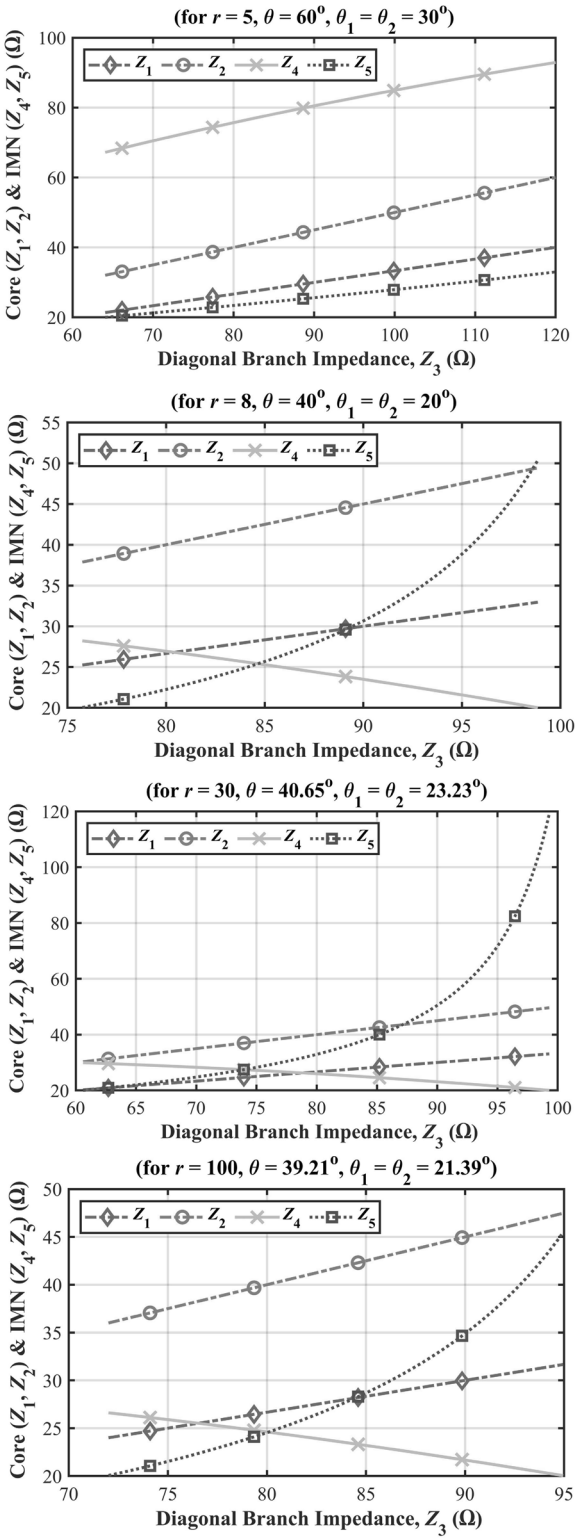

FIGURE 6. Analytically obtained multiple solutions of circuit parameters when $k = 0$ dB and $Z_p = 50$ *ohm*.

c) Determine multiple sets of $Z_c \in [20\Omega, 120\Omega]$ satisfying (11).

d) Obtain G_{eq} and B_{eq} from Eqs.(7) and (8) using the values of Z_i.

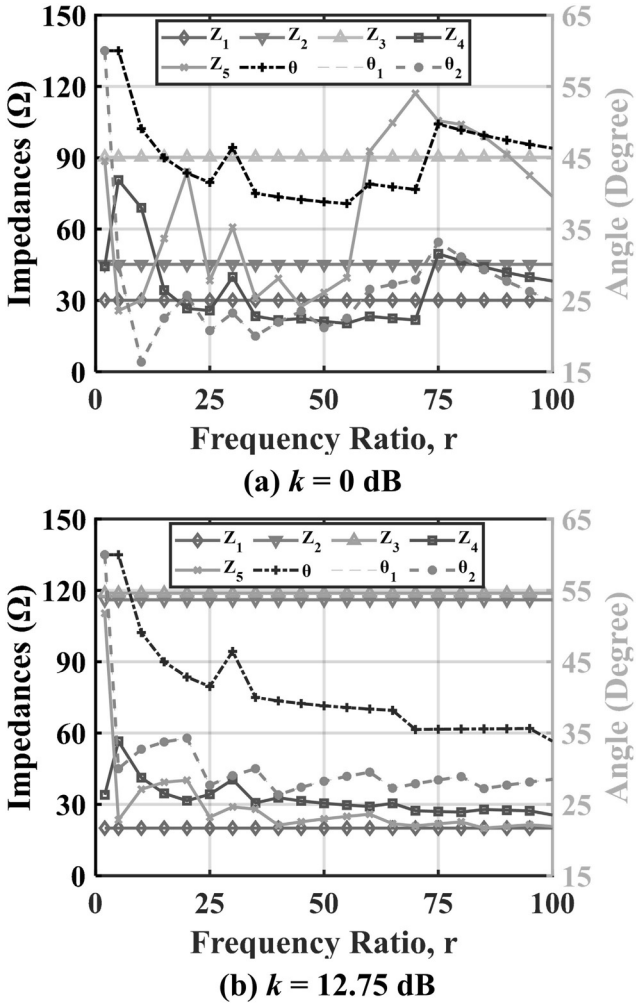

FIGURE 7. Variation of impedances (Z_1, Z_2, Z_3, Z_4, and Z_5) (left axis) and electrical lengths (θ, θ_1, and θ_2) (right axis) Vs unlimited frequency ratio r for power division (a) $k = 0$ dB and $k = 12.75$ dB.

TABLE 1. Dimentions of T-Line Sections(k=0 dB and k=4.77 dB).

Dimensions		1st TL (n = 1)	2nd TL (n = 2)	3rd TL (n = 3)	4th TL (n = 4)	5th TL (n = 5)
W_n (mil)	Equal	356.81	212.19	18.46	138.01	18.46
	Unequal	267.49	72.57	23.62	166.44	21.99
L_n (mil)	Equal	968.38	991.08	1077.32	1010.12	1077.21
	Unequal	1144.28	1209.54	1250.01	1168.86	1252.03

e) Using the calculated G_{eq}, B_{eq}, find Z_{Hi} using (17) and Z_{Vi} using (18) or (19). Check if $20\Omega < Z_{Hi}, Z_{Vi} < 120\Omega$. If yes, store the values of $Z_i, Z_{Hi}, Z_{Vi}, \theta, \theta_1, \theta_2$. Otherwise, we use a different set of Z_c values and repeat step (d).

If the port-matching networks are not identical, the output phase difference may deviate from the ideal value.

C. PROPOSED DIAGONALLY CROSSED TL BASED DBBLC

For the proposed DBBLC structure shown in Fig. 2, P1 serves as the input port, whereas P2 and P3 function as the through and coupled ports, respectively. P4 represents the isolated port. From the even-even, odd-odd, odd-even, and even-odd

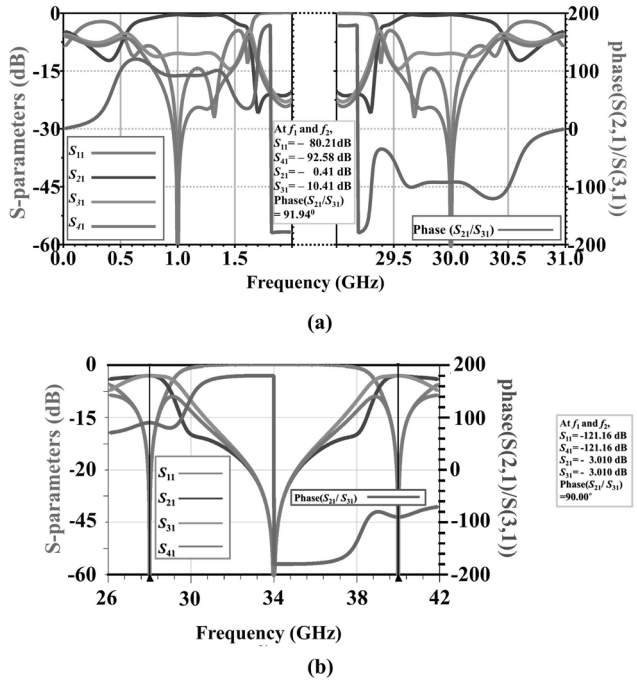

FIGURE 8. The S-parameters S_{11}, S_{21}, S_{31}, and S_{41} (left axis) and phase difference (right axis) for-(a) DBBLC operating at f_1=1 GHz, f_2 = 30 GHz for $(Z_1, Z_2, Z_3) = (20, 80, 112)$ *ohm*, $(Z_{H1}, Z_{H2}, Z_{H3}, Z_{H4}) = (34.78, 39.72, 44.17, 48.27)$ *ohm*, $(Z_{V1}, Z_{V2}, Z_{V3}, Z_{V4}) = (61.26, 59.26, 59.23, 60.03)$ *ohm*, $\theta = 46.45°, \theta_1 = \theta_2 = 40.65°$ (b) DBBLC operating at FR2 of 5G for $(Z_1, Z_2, Z_3) = (36, 54, 108)$ *ohm*, $(Z_{H1} = Z_{H2} = Z_{H3} = Z_{H4}) = 21.67$ *ohm*, $(Z_{V1} = Z_{V2} = Z_{V3} = Z_{V4}) = 89.16$ *ohm*, $\theta = \theta_1 = \theta_2 = 74.12°$.

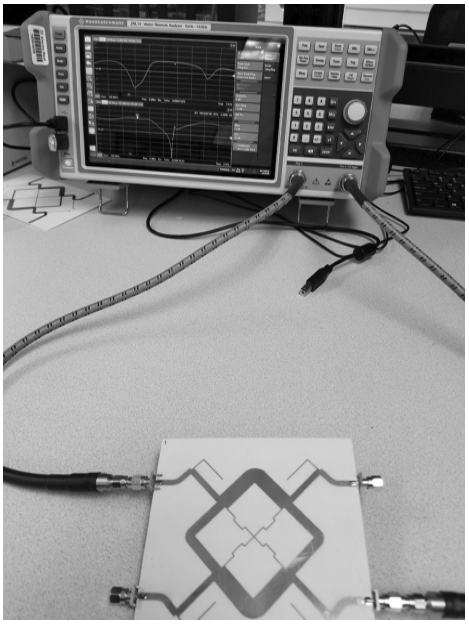

FIGURE 9. Test setup for the measurement of the S-parameters for the fabricated prototype for equal power division ($k = 0$ dB).

equivalent circuits shown in Figs. 4(a)-(d), the equivalent susceptances are found to be as per Eqs. (20)-(23).

$$B_A = \left(\frac{Y_{ee}}{j}\right) = a(Y_1 + Y_2 + Y_3) \tag{20}$$

$$B_B = \left(\frac{Y_{oo}}{j}\right) = \left(-\frac{1}{a}\right)(Y_1 + Y_2 + Y_3) \tag{21}$$

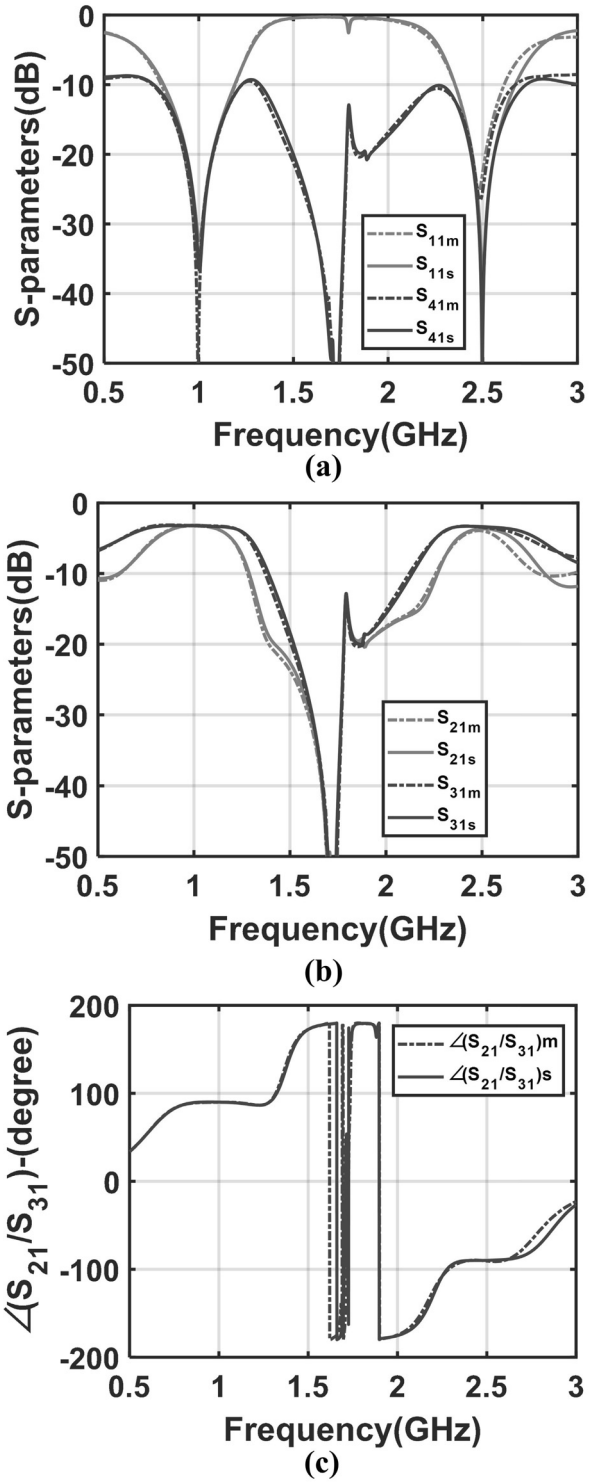

FIGURE 10. The EM simulated (subscript s) vs. measured (subscript m) results-(a) $|S_{11}|$ and $|S_{41}|$ (b) $|S_{21}|$ and $|S_{31}|$ and (c) Phase imbalance for equal ($k = 0$ dB) power division with $r = 2.5$.

$$B_C = \left(\frac{Y_{oe}}{j}\right) = \left(aY_1 - \frac{Y_2}{a} - \frac{Y_3}{a}\right) \tag{22}$$

$$B_D = \left(\frac{Y_{eo}}{j}\right) = \left(-\frac{Y_1}{a} + aY_2 - \frac{Y_3}{a}\right) \tag{23}$$

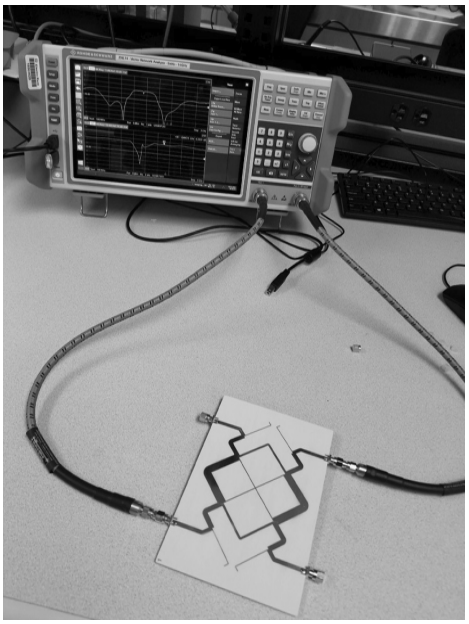

FIGURE 11. Test setup for the measurement of the *S*-parameters for the fabricated prototype for unequal power division ($k = 4.77$ dB).

where $Y_1 = 1/Z_1, Y_2 = 1/Z_2, Y_3 = 1/Z_3$ are the characteristic admittances of the BLC-core TLs. Simplifying (11) for the proposed DBBLC results in the following expression for k.

$$k = \sqrt{\frac{(Y_1 + Y_2 + Y_3)(Y_1 - Y_2)}{Y_2(Y_2 + Y_3)}} \tag{24}$$

It is apparent that k does not depend on θ which facilitates a highly flexible design of IMNs based on a wider range of Y_{eq}. This is the main reason for choosing a crossed TL-based core. Furthermore, considering Z_3 to be a free variable, we can deduce the following from (24) for any value of k:

$$Z_1 = \frac{2}{\{\sqrt{1 + 4k_1(1 + k_1)(1 + k_1)^2} - 1\}} Z_3 \tag{25}$$

$$Z_2 = \frac{Z_3}{k_1} \tag{26}$$

where k_1 parameterizes Z_2 as a function of Z_3.

After exploring various solutions of (25) and (26), a notable relation among the core impedances is discovered- $Z_1 : Z_2 : Z_3 = 2 : 3 : 6$ which is valid for equal power division case ($k = 0$ dB). This substantially reduces the computational complexity of determining the remaining parameters.

Applying (7) and (8) to the proposed DBBLC results in the following expressions:

$$G_{eq} = (1 + a^2)\frac{\sqrt{Y_2(Y_2 + Y_3)(Y_1 - Y_2)(Y_1 + Y_2 + Y_3)}}{a(2Y_2 + Y_3)} \tag{27}$$

$$B_{eq} = \frac{(Y_1 + Y_2 + Y_3)\{(a_1^2 - 1)Y_2 - Y_3\}}{a(2Y_2 + Y_3)} \tag{28}$$

Although k offers a multitude set of Z_1, Z_2, Z_3 values calculated from (25) and (26), the limitations of IMN come

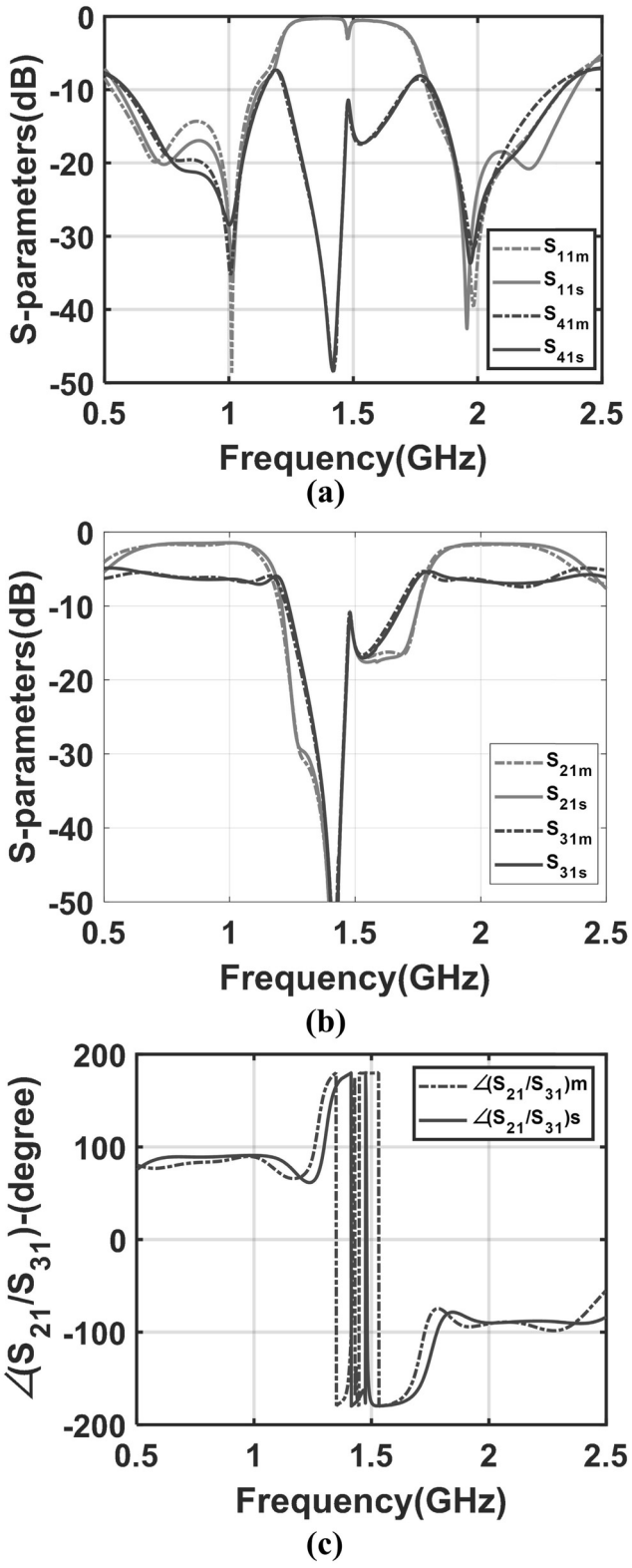

FIGURE 12. The EM simulated (subscript s) vs. measured (subscript m) results-(a) $|S_{11}|$ and $|S_{41}|$ (b) $|S_{21}|$ and $|S_{31}|$ and (c) Phase imbalance for unequal ($k = 4.77$ dB) power division with $r = 2$.

into play because of the dependence of r on G_{eq} and B_{eq} as is evident from (27) and (28). Based on the new equations obtained in II (C), a novel systematic approach to designing the proposed DBBLC is presented in Fig. 5 for equal port impedance ($Z_{p1} = Z_{p2} = Z_{p3} = Z_{p4} = Z_p$). In this case, we can obtain Z_4, Z_5 for the L-section IMN from (17), (18) and (19), where $Z_{H1} = Z_{H2} = Z_{H3} = Z_{H4} = Z_4, Z_{V1} = Z_{V2} = Z_{V3} = Z_{V4} = Z_5$.

Using the proposed design methodology, the theoretical results of a few design examples are shown in Fig. 6 for the equal power division case ($k = 0$ dB). It is observed that multiple design values can be used to design the proposed structure covering a wide range of band ratios, providing immense design flexibility. Moreover, it is apparent from Fig. 7 that r can be practically unlimited based on the appropriate selection of m, p, q and $k_{max} = 18.84$ (12.75 dB), which indicates an extreme power division limit of 94.96% and 5.04% between the through and coupled ports, respectively. The proposed design approach is equally valid for unequal port impedances if the phase error is acceptable [20]. To demonstrate the theory of the proposed design approach, the ideal S-parameters for a representative case are shown in Fig. 8(a). Here, f_1=1 GHz, $f_2 = 30$ GHz, $r = 30$, power division ratio = 10:1 (that is, $k = 10$ dB), port impedances $Z_{p1} = 50\Omega, Z_{p2} = 60\Omega, Z_{p3} = 70\Omega, Z_{p4} = 80\Omega$. The designed DBBLC exhibited excellent performance while maintaining an output phase imbalance of within 1.95°.To design FR2 of 5G, there are multiple design values available for the proposed DBBLC structure based on the novel design approach. The FR2 of 5G includes frequencies ranging from 24.25 GHz to 52.6 GHz. To demonstrate the performance of this design approach of an equal power divider ($k = 0$ dB) DBBLC operating at $f_1 = 28$ GHz and $f_2 = 40$ GHz ($r = 1.43$) which falls under FR2 with port impedances $Z_{p1} = Z_{p2} = Z_{p3} = Z_{p4} = 50\Omega$, the S-parameters are shown in Fig. 8(b), which exhibits the desired performance at $f_1 = 28$ GHz and $f_2 = 40$ GHz.

III. DBBLC PROTOTYPES AND MEASUREMENT

The proposed design methodology for a dual-band port-extended branch-line coupler with equal-power division ($k' = 0$ dB) involves the calculation of the circuit parameters. These parameters, including $Z_1 = 24.91\ \Omega$, $Z_2 = 36.62\ \Omega$, $Z_3 = 119.98\ \Omega$, $Z_4 = 48.70\ \Omega$, $Z_5 = 119.81\ \Omega$, and $k' = 1$ at the first design frequency $f_1 = 1$ GHz, are determined for a port impedance, $Z_p = 50\ \Omega$, using the flowchart illustrated in Fig. 5. The layout used to fabricate the prototype, is presented in Fig. 9, and the physical dimensions are provided in mils (thousandths of an inch) in Table 1. The scattering parameters of the fabricated prototype were measured using a Rohde-Schwarz ZNL14 vector-network analyzer (VNA), as shown in Fig. 9-, and the computer screen displays the measured $|S_{21}|$.

Figs 10(a)-(c) present the electromagnetic (EM) simulated outcomes achieved through Keysight ADS, compared with the measured S-parameter magnitude response. The results exhibit the intended dual characteristic, with measured $|S_{21}|$ and $|S_{31}|$ at -3.16 dB and -3.25 dB, respectively, at 1 GHz, and -3.66 dB and -3.36 dB at 2.5 GHz.

TABLE 2. Comparison with the current state of art dual-band quadrature hybrids.

Refs.	Techniques	Basis of Performance of Fabricated Prototypes										Basis of Features		
		f (GHz)		S-parameters (– dB)				|PD[a]| (°)	|AI[b]| (dB)	FBW[c] (%)	Sizes, $L \times W$	r_{max}[d]	APS[e] (k_{max}[j])	APT[f]
				S_{11}	S_{21}	S_{31}	S_{41}							
[21] IEEE TCAS, 2018	Branch-lines with Open Coupled-lines	EPD[g]	0.75	15.0	3.35	4.00	14.0	89.10	0.34, 0.99	-	$0.25\lambda_0 \times 0.25\lambda_0$ (λ_0 @ 0.75 GHz)	3.4	Yes (4.77)	Yes
			1.42	15.0	3.74	4.10	14.0	89.60	0.73, 1.09	-				
[22] IEEE Access, 2019	Open ended Coupled Lines with Aperture Coupling	EPD[g]	1	25.4	3.59	3.23	24.8	90.94	0.58, 0.22	22.50	$0.65\lambda_0 \times 0.06\lambda_0$ (λ_0 @1.0GHz)	11.7	Yes (6.00)	No
			6	33.5	4.31	4.20	18.7	88.00	1.30, 1.19	4.08				
		UPD[h]	2	14.4	4.08	3.54	19.3	90.71	1.07, 0.53	13.50	$0.60\lambda_0 \times 0.12\lambda_0$ (λ_0 @2.0GHz)			
			4	12.7	5.78	3.18	16.3	93.00	0.22, 2.82	6.38				
[15] IEEE TCAS, 2020	Short/Open-Ended Stubs	EPD[g]	0.9	20.0	3.43	4.07	14.0	89.60	0.42, 1.06	15.03	$0.60\lambda_0 \times 0.27\lambda_0$ (λ_0 @ 0.9 GHz)	2.0	Yes (4.77)	No
			1.8	20.0	3.54	3.67	14.0	90.70	0.53, 0.66	3.89				
[23] IEEE MWCL, 2022	Three coupled microstrip–slotlines	EPD[g]	1	18.5	3.76	3.60	24.2	93.90	0.75, 0.59	12.80	$0.59\lambda_0 \times 0.02\lambda_0$ (λ_0 @1.0GHz)	3.0	No (0)	No
			2	20.7	3.87	3.63	26.6	86.40	0.86, 0.62	13.10				
		EPD[g]	1	21.6	3.33	3.80	30.0	93.80	0.32, 0.79	21.00	$0.39\lambda_0 \times 0.05\lambda_0$ (λ_0 @1.0GHz)			
			3	19.7	3.52	3.96	23.0	88.60	0.51, 0.95	6.70				
This Work	**Diagonally Crossed TLs with Novel Systematic Design**	**EPD[g]**	**1**	**36.4**	**3.23**	**3.21**	**48.4**	**89.92**	**0.22, 0.20**	**31.80**	**$0.40\lambda_0 \times 0.31\lambda_0$ (λ_0 @ 1.0 GHz)**	**inf[i]**	**Yes (12.75)**	**Yes**
			2.5	**22.6**	**3.65**	**3.44**	**25.2**	**90.57**	**0.64, 0.43**	**7.93**				
		UPD[h]	**1**	**39.3**	**1.48**	**6.42**	**35.2**	**88.88**	**0.23, 0.40**	**18.24**	**$0.46\lambda_0 \times 0.34\lambda_0$ (λ_0 @ 1.0 GHz)**			
			2	**33.3**	**1.74**	**6.49**	**29.9**	**90.74**	**0.49, 0.47**	**18.00**				

[a]Phase Difference; [b]Amplitude Imbalance of (S_{21}, S_{31}) from ideal value; [c]Fractional Bandwidth (in terms of ±1dB AI and ±5⁰ PD); [d]Highest supported band ratio; [e]Arbitrary Power Split; [f]Arbitrary Port Termination; [g]Equal Power Division; [h]Unequal Power Division; [i]infinity; [j]Maxmium Power Division Ratio in dB

Additionally, the return loss and isolation loss were both better than 15 dB at both frequencies. For a 10 dB reference, the return loss bandwidths are 368 MHz at f_1 and 318 MHz at f_2, while the isolation loss bandwidths were 462 MHz at f_1 and 473 MHz at f_2. The transmission bandwidth was 257 MHz at f_1 and 153 MHz at f_2. Although the overall magnitude responses of S_{11} and S_{41} shift slightly from the intended second center frequency of 2.5 GHz due to fabrication tolerances, the 10 dB bandwidth supports the simulated regions of operation. Any such shift can be corrected through postfabrication tuning and simulations. Fig. 10(c) shows the simulated and measured phase differences between ports 2 and 3 of the coupler, indicating that the measured results align with the simulated results at both design frequencies. The measured phase differences between the through port and coupled port were determined to be 90.057° at f_1 and −89.873° at f_2, respectively.

In addition, the circuit parameters of a dual-band port-extended branch-line coupler with an unequal-power division ($k' = 4.77$ dB) are calculated for a port impedance of $Z_p = 50\ \Omega$ using the flowchart shown in Fig. 5. At the first design frequency of $f_1 = 1$ GHz, the parameters are determined to be $Z_1 = 31\ \Omega$, $Z_2 = 70\ \Omega$, $Z_3 = 111\ \Omega$, $Z_4 = 43.19\ \Omega$, and $Z_5 = 113.6\ \Omega$. The physical dimensions of the fabricated prototype are listed in mils (thousandths of an inch) in Table 1. The scattering parameters of the designed prototype were measured using the same VNA as shown in Fig. 11, and the measured $|S_{21}|$ was displayed on the computer screen of the VNA.

Figs. 12(a)-(c) display the EM simulated results obtained using the Keysight ADS, along with the measured S-parameter magnitude response. The response exhibits dual-band characteristics as expected, with measured value of $|S_{21}|$ and $|S_{31}|$ as −1.45 dB, −6.37 dB at 1 GHz and −1.59, −6.64 dB at 2 GHz, respectively, with return loss and isolation loss better than 15 dB at both design frequencies. For a 10 dB reference, the return loss bandwidths are 438 MHz at f_1 / 448 MHz at f_2, and the isolation loss bandwidths are 452 MHz at f_1 / 463 MHz at f_2, with transmission bandwidths of 236 MHz at f_1 / 253 MHz at f_2. Although the overall magnitude responses of S_{11} and S_{41} shift slightly from the intended second center frequency of 2 GHz owing to fabrication tolerances, the 10 dB bandwidth still supports the proposed/simulated regions of operation. Post-fabrication tuning coupled with simulation can be used to correct this shift if desired. Fig. 12(c) shows the simulated and measured phase differences between ports 2 and 3 of the coupler. The measured results correlate well with the simulated results at both design frequencies. The measured phase differences between the through port and coupled port were 90.18° at f_1, −89.81° at f_2, respectively.

To highlight the novelty of this work further, the % FBW related to these parameters, as well as other salient features, are summarized in Table 2 and compared to the current

state-of-the-art methods. Overall, the measured results demonstrat the outstanding performance of different DBBLC configurations that meet all the goals that a practical quadrature coupler will be required during deployment in the field.

IV. CONCLUSION

This study introduces a new systematic design approach for a dual-band branch-line coupler (DBBLC) that enables the achievement of various power division ratios at different band ratios with arbitrary port terminations simultaneously, utilizing crossed lines inside the coupler core and L-section IMNs. The two fabricated prototypes demonstrated design flexibility, as outlined in the proposed flowchart. Moreover, the excellent agreement between the EM simulation of the DBBLCs and the measured responses from the prototypes validates the proposed novel design approach.

ACKNOWLEDGMENT

The authors acknowledge that ChatGPT 3.5 (https://chat.openai.com/) was used in some of the paragraphs to improve text vocabulary.

REFERENCES

[1] R. E. Collin, *Foundations for Microwave Engineering*, 2nd ed. New Delhi, India: Wiley, 2005, pp. 432–434.

[2] H. Hashemi and A. Hajimiri, "Concurrent multiband low-noise amplifiers-theory, design, and applications," *IEEE Trans. Microw. Theory Techn.*, vol. 50, no. 1, pp. 288–301, Jan. 2002.

[3] A. I. Omi, Md. S. I. Sagar, M. M. H. Sajeeb, B. Younes, T. Karacolak, and P. Sekhar, "A new analytically designed UWB microstrip patch antenna for future 5G and 6G applications," in *Proc. United States Nat. Committee URSI Nat. Radio Sci. Meeting (USNC-URSI NRSM)*, Jan. 2023, pp. 62–63.

[4] A. M. Zaidi, M. T. Beg, B. K. Kanaujia, K. Rawat, S. Kumar, K. Rambabu, S. P. Singh, and A. Lay-Ekuakille, "A dual-band rat-race coupler for high band ratio wireless applications," *IEEE Trans. Instrum. Meas.*, vol. 70, pp. 1–6, 2021.

[5] A. M. Zaidi, M. T. Beg, B. K. Kanaujia, K. Srivastava, and K. Rambabu, "A dual band branch line coupler with wide frequency ratio," *IEEE Access*, vol. 7, pp. 25046–25052, 2019.

[6] Y. X. Zhou, L. Xu, F. Wei, and T. Feng, "A wideband balanced filtering coupled-line coupler with improved directivity based on coupled microstrip–slotline," *Microw. Opt. Technol. Lett.*, vol. 66, no. 2, Feb. 2024, Art. no. e34049.

[7] M. E. Nouri, S. Roshani, M. H. Mozaffari, and A. Nosratpour, "Design of high-efficiency compact Doherty power amplifier with harmonics suppression and wide operation frequency band," *Int. J. Electron. Commun.*, vol. 118, May 2020, Art. no. 153168.

[8] S. S. Gao, S. Sun, and S. Xiao, "A novel wideband bandpass power divider with harmonic-suppressed ring resonator," *IEEE Microw. Wireless Compon. Lett.*, vol. 23, no. 3, pp. 119–121, Mar. 2013.

[9] H. Boutayeb, P. R. Watson, W. Lu, and T. Wu, "Beam switching dual polarized antenna array with reconfigurable radial waveguide power dividers," *IEEE Trans. Antennas Propag.*, vol. 65, no. 4, pp. 1807–1814, Apr. 2017.

[10] B. Younes, A. I. Omi, Md. S. I. Sagar, M. M. H. Sajeeb, T. Karacolak, and P. Sekhar, "A physically compact coplanar waveguide (CPW)-fed flexible antenna for mmWave 5G applications," in *Proc. 12th Int. Conf. Electr. Comput. Eng. (ICECE)*, Dec. 2022, pp. 196–199.

[11] A. I. Omi, Ahammad, M. H. Maktoomi, M. A. Maktoomi, and P. K. Sekhar, "Miniaturized wideband three-way power dividers with arbitrary band ratio using a new analytical design technique," *IEEE Access*, vol. 11, pp. 72148–72158, 2023.

[12] A. I. Omi, R. Islam, M. A. Maktoomi, C. Zakzewski, and P. Sekhar, "A novel analytical design technique for a wideband Wilkinson power divider using dual-band topology," *Sensors*, vol. 21, no. 19, p. 6330, Sep. 2021.

[13] M.-J. Park and B. Lee, "Dual-band, cross coupled branch line coupler," *IEEE Microw. Wireless Compon. Lett.*, vol. 15, no. 10, pp. 655–657, Oct. 2005.

[14] H. Chang, T. Lim, K. C. Dimitrov, and Y. Lee, "Dual-band branch-line coupler based on crossed lines for arbitrary power-split ratios," *Sensors*, vol. 22, no. 15, p. 5527, Jul. 2022.

[15] W. Feng, X. Duan, Y. Shi, X. Y. Zhou, and W. Che, "Dual-band branch-line couplers with short/open-ended stubs," *IEEE Trans. Circuits Syst. II, Exp. Briefs*, vol. 67, no. 11, pp. 2497–2501, Nov. 2020.

[16] M. A. Maktoomi, M. S. Hashmi, and F. M. Ghannouchi, "Systematic design technique for dual-band branch-line coupler using T- and pi-networks and their application in novel wideband-ratio crossover," *IEEE Trans. Compon., Packag., Manuf. Technol.*, vol. 6, no. 5, pp. 784–795, May 2016.

[17] L. Xia, J.-L. Li, B. A. Twumasi, P. Liu, and S.-S. Gao, "Planar dual-band branch-line coupler with large frequency ratio," *IEEE Access*, vol. 8, pp. 33188–33195, 2020.

[18] L. K. Yeung, "A compact dual-band 90° coupler with coupled-line sections," *IEEE Trans. Microw. Theory Techn.*, vol. 59, no. 9, pp. 2227–2232, Sep. 2011.

[19] C.-H. Yu and Y.-H. Pang, "Dual-band unequal-power quadrature branch-line coupler with coupled lines," *IEEE Microw. Wireless Compon. Lett.*, vol. 23, no. 1, pp. 10–12, Jan. 2013.

[20] M. A. Maktoomi, M. S. Hashmi, and F. M. Ghannouchi, "A dual-band port-extended branch-line coupler and mitigation of the band-ratio and power division limitations," *IEEE Trans. Compon., Packag., Manuf. Technol.*, vol. 7, no. 8, pp. 1313–1323, Aug. 2017.

[21] W. Feng, Y. Zhao, W. Che, H. Chen, and W. Yang, "Dual-/tri-band branch line couplers with high power division isolation using coupled lines," *IEEE Trans. Circuits Syst. II, Exp. Briefs*, vol. 65, no. 4, pp. 461–465, Apr. 2018.

[22] L. Gao, S. Y. Zheng, W. Hong, and Y. Li, "Tight coupling dual-band coupler with large frequency ratio and arbitrary power division ratios over two bands," *IEEE Access*, vol. 7, pp. 184489–184499, 2019.

[23] X. Zhao, F. Zhu, K. Fan, G. Q. Luo, and K. Wu, "A compact dual-band coupler with coupled microstrip–slotlines," *IEEE Microw. Wireless Compon. Lett.*, vol. 32, no. 4, pp. 277–280, Apr. 2022.

[24] F. Wei, L. Y. Qiao, Y. Han, X.-B. Zhao, L. Xu, R. Li, and X. W. Shi, "A balanced filtering directional coupler based on slotline using asymmetric parallel loaded branches," *IEEE Trans. Compon., Packag., Manuf. Technol.*, vol. 12, no. 7, pp. 1222–1231, Jul. 2022.

[25] R. Sinha and A. De, "Comments on 'An analytical design method for a novel dual-band unequal coupler with four arbitrary terminated resistance,'" *IEEE Trans. Ind. Electron.*, vol. 64, no. 5, pp. 4068–4069, May 2017.

[26] Y. Wu, S. Y. Zheng, S.-W. Leung, Y. Liu, and Q. Xue, "An analytical design method for a novel dual-band unequal coupler with four arbitrary terminated resistances," *IEEE Trans. Ind. Electron.*, vol. 61, no. 10, pp. 5509–5516, Oct. 2014.

[27] R. Sinha, "Comments on 'A dual-band port-extended branch-line coupler and mitigation of the band-ratio and power division limitations,'" *IEEE Trans. Compon., Packag., Manuf. Technol.*, vol. 9, no. 6, pp. 1203–1205, Jun. 2019.

AHAMMAD (Graduate Student Member, IEEE) was born in Dhaka, Bangladesh. He received the B.Sc. degree in electrical and electronic engineering from Islamic University of Technology, Dhaka, in 2008, and the M.Sc. degree in electrical and electronic engineering from Bangladesh University of Engineering and Technology, Dhaka, in 2014. He was a Faculty Member with the Electrical and Electronic Engineering Department, Ahsanullah University of Science and Technology, from 2009 to 2019. He has been a Teaching Assistant with Washington State University Vancouver, since Fall 2023. He is currently doing research on radio-frequency/microwave circuits and systems for wireless communications. His research interests include RF/Microwave front-end passive circuit design, RF low noise amplifier, and power amplifier design.

ASIF IFTEKHAR OMI (Student Member, IEEE) was born in Dhaka, Bangladesh. He received the B.Sc. degree (Hons.) in electrical and electronic engineering from Bangladesh University of Engineering and Technology, Dhaka, in 2014, and the M.S. degree from Washington State University Vancouver, Vancouver, WA, USA, in 2022. He is currently pursuing the Ph.D. degree with the University of Florida, Gainesville, FL, USA. From 2014 to 2015, he was a Lecturer with Bangladesh University of Business and Technology, where he taught a few undergraduate courses, such as electromagnetics, numerical methods and continuous signals, and supervised hardware laboratories. From 2015 to 2020, he was with the Project Implementation Team, Dhaka Power Distribution Company Ltd., as a Sub-Divisional Engineer, where he developed adequate knowledge in the areas of signaling flow and protocols, coupling between protective relays, electromagnetic transmission, SCADA integration, UHF antenna systems, substation automation systems, fiber optic multiplexer, and miscellaneous tele-protection devices with the received hands-on training from ABB Ltd., Switzerland, and Schneider Electric Ltd., Germany. From 2021 to 2022, he joined Washington State University as a Teaching Assistant, where his entire research endeavor was on microwave front-end passive circuit design. Since Spring 2023, he has been a Graduate Research Assistant with the Analog/Mixed Signal Laboratory, University of Florida. His current research interest includes RF integrated circuits.

MOHAMMAD H. MAKTOOMI (Graduate Student Member, IEEE) received the B.Engg. degree in electronics and communication from Jamia Millia Islamia, New Delhi, India, in 2015, and the M.S. degree in electrical engineering from Washington State University Vancouver, Vancouver, WA, USA, in 2020. He is currently pursuing the Ph.D. degree with the University of California at Irvine, Irvine, CA, USA. From 2016 to 2017, he was an Intern and a Research Assistant with IIIT Delhi, New Delhi, where he was involved in research on passive RF/microwave circuits. In Summer 2019, he joined the Research and Development Department, Wolfspeed Inc., Morgan Hill, CA, USA, as a RF Engineering Intern, where he was involved in Doherty power amplifier module design and Python programming-based load-pull data analysis. His current research interest includes RF/millimeter-wave integrated circuits. He was a recipient of the 2022 IEEE Custom Integrated Circuits Conference (CICC) Education Award. He serves as a Reviewer for IEEE TRANSACTIONS ON CIRCUITS AND SYSTEMS—II: EXPRESS BRIEFS, *IET Microwaves, Antennas & Propagation*, *Electronics Letters* (IET), and *Progress in Electromagnetics Research*.

MOHAMMAD A. MAKTOOMI (Member, IEEE) was born in Muzaffarpur, India. He received the B.Tech. degree in electronics engineering from Aligarh Muslim University, India, in 2009, and the M.Tech. and Ph.D. degrees in electronics and communication engineering from the Indraprastha Institute of Information Technology, Delhi (IIIT Delhi), India, in 2016. He is currently an Assistant Professor with the Department of Electrical and Computer Engineering, Virginia Military Institute, USA. Previously, he has held faculty positions with The University of Scranton, USA, Hindustan College of Science and Technology, and Aligarh Muslim University, India. His research interests include the design and analysis of radio-frequency/microwave circuits and systems for wireless communications and the Internet of Things applications. He received the University of Calgary Eyes High Postdoctoral Fellowship, the Best Student Paper Award at IEEE MWSCAS 2016, and the DST Science and Engineering Research Board (SERB) Travel Grant, and was a winner of the Microstrip Bandpass Filter Design Competition held during IEEE IMaRC 2015. He is a reviewer of several IEEE TRANSACTIONS and journals and an Academic Editor of *PLOS One* journal.

PRAVEEN K. SEKHAR (Member, IEEE) was an Assistant Professor with Washington State University (WSU) Vancouver, in 2011. Prior to that, he worked as a Postdoctoral Fellow with the Sensors and Electrochemical Devices Group, Los Alamos National Laboratory (LANL), Los Alamos, NM, USA. He is currently an Associate Professor with the School of Engineering and Computer Science, WSU Vancouver. His research interests include the Internet of Things (IoT) encompassing sensors and microwave devices. He was a recipient of the Alexander von Humboldt Fellowship and is an Associate Editor of *Journal of the Electrochemical Society*.